Digest Journal of Nanomaterials and Biostructures Vol. 15, No. 1, January - March 2020, p. 185 - 195

ACETYLACETONATE HYDROUS ZIRCONIUM(IV) COMPLEXES SUPPORTED ON HYDROPHILIC POLYMERS AS NEW SELECTIVE GROWTH PRECURSORS OF MONOCLINIC AND TETRAGONAL ZIRCONIUM OXIDE NANOCRYSTALS

J. A. PÉREZ-TAVARES[a], R. PATAKFALVI[a,*], L. ORTIZ-FRADE[b], C. FRAUSTO-REYES[c], Q. E. SAAVEDRA-ARROYO[d], H. PÉREZ-LADRÓN DE GUEVARA[a], J. CASTAÑEDA-CONTRERAS[a], V. F. MARAÑÓN-RUIZ[a]

[a]*Los Lagos University Center, University of Guadalajara, Lagos de Moreno, Jalisco, Mexico*

[b]*Center of Research and Technological Development in Electrochemistry S.C. Parque Tecnológico Querétaro, Sanfandila, Pedro de Escobedo, C.P. 76703. Querétaro, Mexico*

[c]*Optical Research Center, Aguascalientes Campus, Aguascalientes, Mexico*

[d]*Technological Institute of Irapuato, Materials Science Department, Irapuato, Guanajuato, Mexico*

Pure ZrO_2 nanocrystals were successfully prepared from three new complexes of hydrous zirconium acetylacetonate ($[Zr_2(AcAc)\bullet 4H_2O]_2$, $[Zr_2(AcAc)\text{-}PEI\bullet nH_2O]_2$ and $[Zr_2(AcAc)\text{-}PDDAC\bullet nH_2O]_2$), obtained using solvothermal synthesis. The addition of poly(ethyleneimine) (PEI) and poly(diallyldimethylammonium chloride) (PDDAC) hydrophilic polymers as stabilizing agents, had impact on the size and crystalline phase of the calcinated products within a range of 300 to 800 °C, obtaining ZrO_2 nanoparticles with tetragonal and/or monoclinic structure and diameters of 5 to 20 nm. The synthesized precursor complexes and ZrO_2 were characterized by thermogravimetry (TGA), differential scanning calorimetry (DSC), X-ray diffraction (XRD), UV-Vis spectroscopy, Fourier transformed infrared spectroscopy (FT-IR/FIR) and Raman spectroscopy.

(Received October 15, 2019; Accepted March 10, 2020)

Keywords: Zirconium oxide, FT-IR spectroscopy, Raman spectroscopy, UV-Vis spectroscopy, Energy band gap, X-ray analysis, Nanocrystals, Thermal decomposition, Inorganic materials, Chemical synthesis

1. Introduction

Nanometric-sized zirconia has attracted considerable attention due to its specific properties as high melting point, chemical inertness, high refractive index, wide bandgap, high dielectric constant, and high electrical resistivity [1], as well as other potential applications in transparent optical devices, electrochemical capacitor electrodes, oxygen sensors, fuel cell electrolytes, catalysts and advanced ceramics [2-4].

ZrO_2 is polymorphic in nature with several crystal structures at different temperatures that allow controlling the grain size or order to tune specific properties for different applications [5]: monoclinic (temperature below 1175 °C), tetragonal (1175-2370 °C) and cubic (2370-2680 °C). Pure zirconium oxide is considered the stable form at room temperature is a monoclinic phase. However, as temperature treatment is increased, the amorphous ZrO_2 precursors undergo a preliminary transformation from the tetragonal phase to the monoclinic phase at higher temperatures (~600 °C), undergoing a complete transformation above 800 °C. The metastable tetragonal phase during the crystallization of amorphous hydrous zirconia in nanocrystalline ZrO_2 is relevant for ceramic and catalytic applications [6-8]. Ultrafine zirconium particles have been

* Corresponding author: rpatakfalvi@culagos.udg.mx

synthesized using several methods, such as solvothermal synthesis [8], sol-gel [9-11], decomposition of zirconium salts [12], sonochemical synthesis [7], precipitation [6,11,13], electron-beam physical vapor deposition, plasma pulverization [14-15], combustion [16], ultrasonically assisted hydrothermal synthesis [17] and gas-phase reactions [18].

A wide variety of zirconium compounds have been used as precursors for the synthesis of ZrO_2 nanomaterials with different sizes and crystalline phases: $Zr(AcAc)_4$-citric acid (12.1-27.9 nm, tetragonal and monoclinic) [4, 19], b-ketoiminato zirconium complexes (orthorhombic) [20], $[Zr(AcAc)_3(H_2O)_2]Cl$ (40-50 nm, tetragonal and monoclinic) [5] and $[Zr(AcAc)_3(H_2O)_2]NO_3$ (10-30 nm cubic) [21], tetrakis(dimethylamido)zirconium complex (cubic, orthorhombic and monoclinic) [22], $Zr(Cp)(^tBuDAD)(O^iPr)$, Zr(MeCp)(TMEA), and $Zr(Me_5Cp)(TEA)$ (^tBuDAD = N,N-bis(tertbutyl)ethene-1,2-diaminato, TMEA = tris[2-(methylamino)ethyl]aminate, TEA = triethoanolaminate) (tetragonal and monoclinic) [23], $[Zr(HAP)_3(H_2O)_2](NO_3)$ (HAP = tris-2-hydroxyacetophenato) (30-40 nm, cubic) [24].

In this study, we present the controllable synthesis of tetragonal and/or monoclinic zirconia nanocrystals by introducing a complex of hydrous zirconium acetylacetonate as new selective growth precursor. The effects of particle size were also investigated, using poly (ethyleneimine) (PEI) and poly (diallyldimethylammonium chloride) (PDDAC) polymers, which served as stabilizers for the production of a homogeneous gel during the solvothermal synthesis of this complex, obtaining ZrO_2 with crystallite sizes of 5 to 20 nm.

2. Materials and methods

2.1. Materials

Zirconium (IV) acetylacetonate ($Zr(AcAc)_4$), poly(ethyleneimine) solution (PEI) (M_w 750,000, 50 % (w/v) in H_2O), poly (diallyldimethylammonium chloride) solution (PDDAC) (average M_w 200,000-350,000 (medium molecular weight), 20 wt. % in H_2O) and triethylamine were purchased from Aldrich and used as received, without further purification.

2.2. Synthesis of ZrO_2 nanocrystals

Acetylacetonate hydrous zirconium(IV) complex was synthesized by solvothermal treatment of $Zr(AcAc)_4$ with triethylamine and methanol in the presence and the absence of hydrophilic polymers (3% v/v) PEI and PDDAC as stabilizers. The synthetic pathway is shown in Scheme 1.

In the typical synthesis, 6.4 mmol (3.12 g) of $Zr(AcAc)_4$ was dissolved in methanol or in a methanolic solution of the PEI or PDDAC polymers (32.0 mL) to form a mixed solution. Then 32.0 mmol (4.46 mL) of triethylamine was added to the solution dropwise, stirring moderately and put into an Ace pressure tube (48.0 mL capacity), where it was maintained for 8 h at 120 ºC. Without any polymers, amorphous yellow crystals were obtained ($[Zr_2(AcAc)\bullet 4H_2O]_2$), which were then filtered and washed with methanol until the filtrate became clear. Using PEI or PDDAC, homogenous yellow gel was formed ($[Zr_2(AcAc)\text{-}PEI\bullet nH_2O]_2$ or $[Zr_2(AcAc)\text{-}PDDAC\bullet nH_2O]_2$) and then centrifuged and washed with methanol until a clear supernatant was obtained. The resulting yellow products were dried at 80 ºC for 24 h and then crushed into a fine powder. The powdered samples of $[Zr_2(AcAc)\bullet 4H_2O]_2$, $[Zr_2(AcAc)\text{-}PEI\bullet nH_2O]_2$ and $[Zr_2(AcAc)\text{-}PDDAC\bullet nH_2O]_2$ were separated into different parts, then calcinated at 300, 400, 500, 600, 700 or 800 ºC for 5 h in air, before being cooled to room temperature.

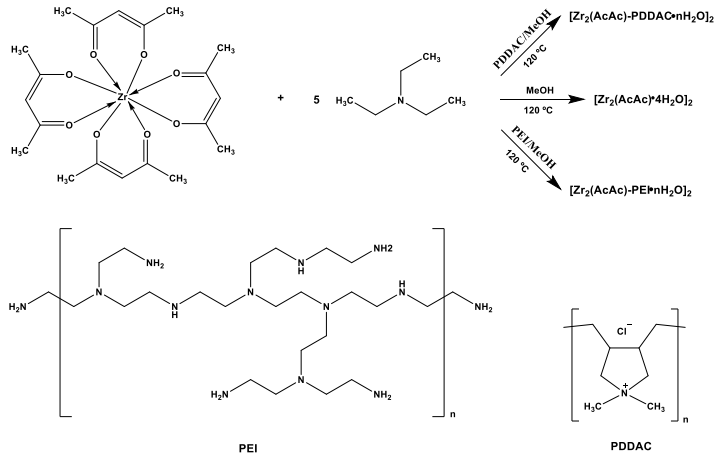

Scheme 1. Synthetic pathway of $[Zr_2(AcAc)•4H_2O]_2$, $[Zr_2(AcAc)\text{-}PEI•nH_2O]_2$ and $[Zr_2(AcAc)\text{-}PDDAC•nH_2O]_2$.

2.3. Characterization

Thermal analyses were carried out using TG/DSC Q20TA/Q600-TA Instruments thermal analyzer in a dry air atmosphere (flow rate of 20 mL min^{-1}, ambient pressure, heating rate 10 °C min^{-1} with a temperature range from 25 to 800 °C) using approximately 15 mg of compounds. Infrared spectroscopic measurements were performed on a Frontier FT-IR/FIR spectrometer (PerkinElmer; DTGS detector; KBr beamsplitter for mid-IR and aluminum grid/polypropylene beamsplitter for far-IR), using attenuated total reflection (ATR) or KBr disc technique. The diffuse reflectance spectra of the powders were obtained using an Ocean Optics QE65000 spectrophotometer with an ISP-30R integrating sphere. The Raman spectra of the samples were obtained by placing them on an aluminum substrate and then under a DM LM microscope (Leica) integrated into the Raman system (Renishaw 1000B). The Raman system was calibrated with a silicon semiconductor using the Raman peak at 520 cm^{-1}. The excitation wavelength was 830 nm, and the laser beam was focused (spot size of approximately 2 mm) on the surface of the sample with a 50x objective. The laser power irradiation over the samples was approximately 10 mW.

The XRD patterns were recorded from 10º to 80º on a PANalytical X-ray diffractometer (Model Empyrean) with monochromatized Cu Kα radiation (λ = 1.5406 Å). Crystallite sizes (D_c) were calculated from the line broadening of the X-ray diffraction peaks, applying the Debey–Scherrer equation (1) [2,25],

$$D_c = \frac{k\lambda}{\beta cos\theta} \quad (1)$$

where β is the breadth of the observed diffraction line at its half-intensity maximum (FWHM), k is the so-called shape factor, which usually takes a value of about 0.9, λ is the wavelength of X-ray source used in XRD and θ is the angle of reflection.

3. Results and discussion

3.1. Thermal analysis

Hydrous zirconium acetylacetonate complexes were characterized by TGA, see Fig. 1. In the case of the $[Zr_2(AcAc)•4H_2O]_2$ complex, the TGA curve presents two well-defined degradation steps: the first, occurring in the temperature range of 25-150 °C can be attributed to the loss of water molecules and the degradation of the acetylacetonate ligand. The complete decomposition of the acetylacetonate complex [20] is observed in the temperature range of 150-650 °C, during the second stage. The total weight loss for the $[Zr_2(AcAc)•4H_2O]_2$ complex was around 30%, leaving a

large amount of residual mass (70%) due to the formation of ZrO_2. With these results, the presence of two zirconium nuclei per molecule of acetylacetonate is proposed, which suggests similar composition to hydrous zirconia, based on tetramers of Zr(IV), molecules of coordination water, hydroxyl groups and oxygen atoms $[Zr_2(AcAc)\bullet 4H_2O]_2 \rightarrow [Zr_4O_6(OH)_2(AcAc)_2]$ [26].

In the case of complexes stabilized with PEI and PDDAC, two degradation steps were also observed around 25 to 100 °C and 100 to 500 °C with a total weight loss of 52% and 28%, respectively. The residual mass of these complexes varied within a range of 48-72% presumably due to ZrO_2 formation. This implies that the nuclei of Zr(IV) have a greater affinity for the PEI polymer compared to PDDAC, which results in a complex with a higher percentage of loss of mass. However, the $[Zr_2(AcAc)\bullet 4H_2O]_2$ complex present high thermal stability in comparison with $[Zr_2(AcAc)\text{-}PEI\bullet nH_2O]_2$ and $[Zr_2(AcAc)\text{-}PDDAC\bullet nH_2O]_2$. Although an initial weight loss is observed, it should be taken into account that the complexes could not be sublimated until their decomposition temperatures of (350-650 °C) were reached and, initial weight loss can be attributed to the sublimation of the acetylacetonate ligand [20,27].

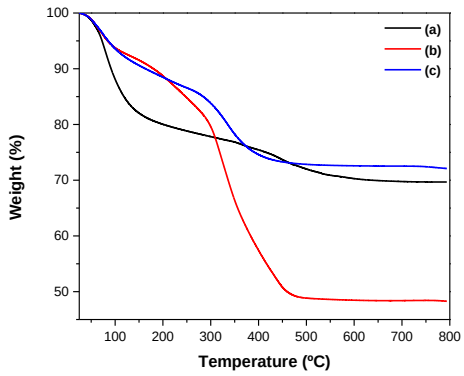

Fig. 1. TG curves of complexes: (a) $[Zr_2(AcAc)\bullet 4H_2O]_2$, (b) $[Zr_2(AcAc)\text{-}PEI\bullet nH_2O]_2$ and (c) $[Zr_2(AcAc)\text{-}PDDAC\bullet nH_2O]_2$.

The recorded DSC curves (Fig. 2) for the acetylacetonate complexes suggest the decomposition of Zr(IV)-AcAc by means of an endothermic weight loss process that maximizes ($[Zr_2(AcAc)\bullet 4H_2O]$) at 90 °C, ($[Zr_2(AcAc)\text{-}PEI\bullet nH_2O]_2$) at 78 °C and ($[Zr_2(AcAc)\text{-}PDDAC\bullet nH_2O]_2$) at 85 °C. This endothermic process is related to the dehydration of the sample as well as the partial decomposition of acetylacetonate. Subsequently, exothermic processes present themselves ($[Zr_2(AcAc)\bullet 4H_2O]$) occurs at 530 °C, ($[Zr_2(AcAc)\text{-}PEI\bullet nH_2O]_2$) at 234, 350, 375, 447 °C and ($[Zr_2(AcAc)\text{-}PDDAC\bullet nH_2O]_2$) at 342 °C, resulting from the decomposition/oxidation of organic matter and the crystallization of tetragonal zirconia nanocrystals during heating [5,28-30].

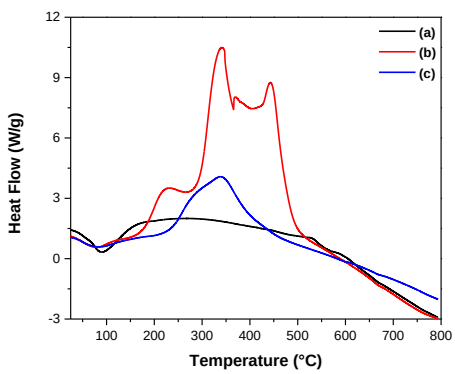

Fig. 2. DSC curves of complexes: (a) $[Zr_2(AcAc)\bullet 4H_2O]_2$, (b) $[Zr_2(AcAc)\text{-}PEI\bullet nH_2O]_2$ and (c) $[Zr_2(AcAc)\text{-}PDDAC\bullet nH_2O]_2$.

3.1.2. X-ray diffraction analysis

The X-ray diffraction patterns of zirconium oxides synthesized under different conditions are presented in Fig. 3, respectively, as a function of the stabilizers and temperature treatment. XRD patterns for the zirconium complexes not calcined do not indicate crystallinity, showing a broad peak near to the strongest diffraction peaks of the tetragonal and monoclinic phases, that why this is not presented here.

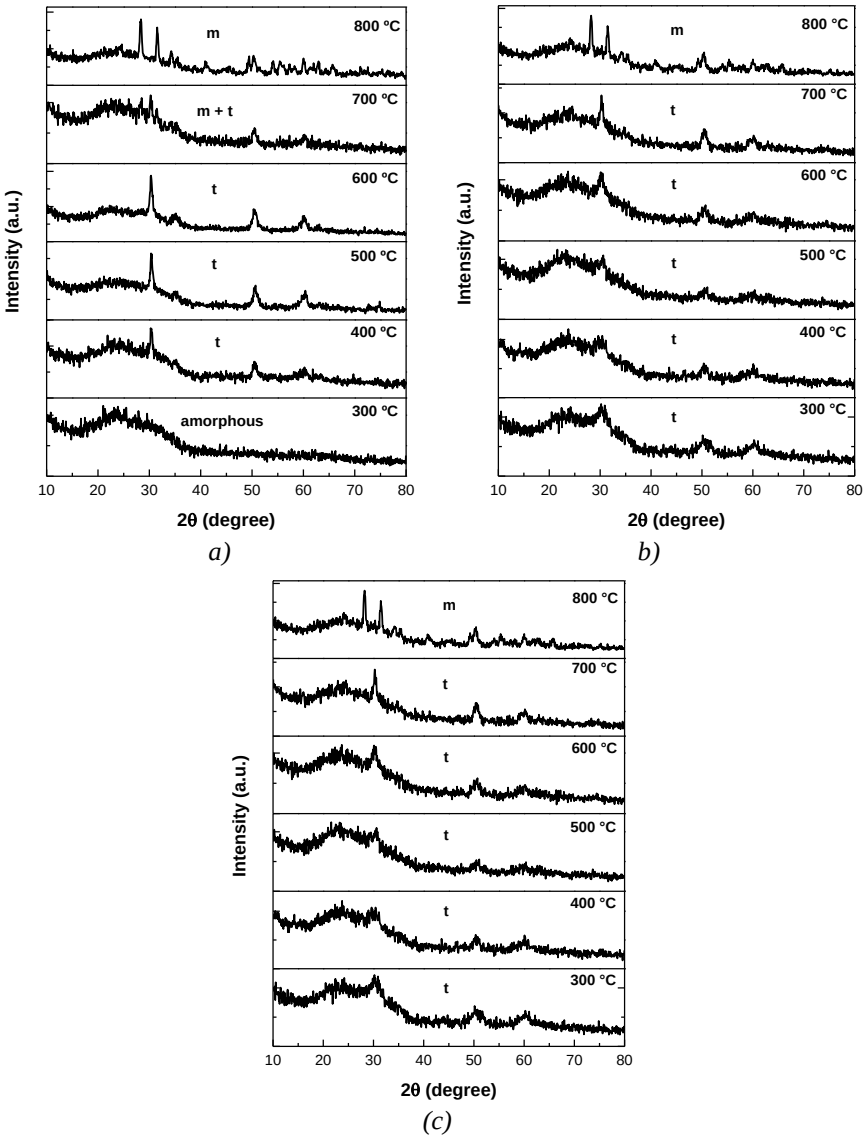

Fig. 3. XRD patterns of ZrO_2 prepared from (a) $[Zr_2(AcAc)\bullet 4H_2O]_2$, (b) $[Zr_2(AcAc)\text{-}PEI\bullet nH_2O]_2$ and (c) $[Zr_2(AcAc)\text{-}PDDAC\bullet nH_2O]_2$.

Fig. 3a shows the XRD for the powders calcined at 300-800 °C, prepared from the $[Zr_2(AcAc)\bullet 4H_2O]_2$ complex. This figure indicates that at 800 °C a monoclinic phase (m) is obtained. At 700 °C, a combination of the monoclinic and tetragonal (t) zirconia phase is produced. When the calcination temperature was reduced from 600 to 400 °C, only the t phase was obtained, whereas below 300 °C amorphous zirconia is detected. Moreover, the XRD shown in Fig. 3b and 3c of heat-treated products obtained from the zirconium complexes stabilized using PEI and PDDAC showed that at 800 °C, the (m) phase is produced for $[Zr_2(AcAc)\text{-}PEI\bullet nH_2O]_2$. In

the case of $[Zr_2(AcAc)\text{-}PDDAC\bullet nH_2O]_2$, around at 700 to 800 °C a combination of m and t phase is obtained. Below the previously mentioned temperatures $[Zr_2(AcAc)\text{-}PEI\bullet nH_2O]_2$ and at 600 to 300 °C $[Zr_2(AcAc)\text{-}PDDAC\bullet nH_2O]_2$), t phase was obtained for both of the original complexes. The distinctive characteristic peaks for the tetragonal phase occur at 2θ = 30.2º, 34.9º, 50.6º and 60.08º for the reflections (1 0 1), (0 0 2), (2 0 0) and (2 1 1) [4,7,11]. Therefore, all the XRD patterns for the samples calcinated at 400-600 °C ($[Zr_2(AcAc)\bullet 4H_2O]_2$), 300-700 °C ($[Zr_2(AcAc)\text{-}PEI\bullet nH_2O]_2$) and 300-600 °C ($[Zr_2(AcAc)\text{-}PDDAC\bullet nH_2O]_2$) were catalogued as at the tetragonal zirconia phase. This is very similar to the values in the literature [4,7,11] and no impurities of $Zr(AcAc)_4$ were found in the X-ray diffraction pattern.

Crystallite sizes (Table 1) of the products prepared from the $[Zr_2(AcAc)\text{-}PEI\bullet nH_2O]_2$ and $[Zr_2(AcAc)\text{-}PDDAC\bullet nH_2O]_2$ complexes, calculated using Scherrer's formula (FWHM of (1 0 1)), presented reduced values for products calcined at low temperatures. As apparent in Table 1, the average crystallite size of all the products fell between 5 and 20 nm. XRD results also indicated that the phase of the products calcined at 300-700 °C for PEI and at 300-600 °C for PDDAC was solely tetragonal. In contrast, products obtained from the $[Zr_2(AcAc)\bullet 4H_2O]_2$ complex did not show variations in crystallite size when the calcination temperature decreased, as the average size was 18 nm, confirming the impact of PEI and PDDAC stabilizers on particle size.

Table 1. The crystallite size of the different samples calculated by the Scherrer equation.

Calcination temperature (°C)	**$[Zr_2(AcAc)\bullet 4H_2O]_2$**		**$[Zr_2(AcAc)\text{-}PEI\bullet nH_2O]_2$**		**$[Zr_2(AcAc)\text{-}PDDAC\bullet nH_2O]_2$**	
	Crystallite size (nm)	Phase	Crystallite size (nm)	Phase	Crystallite size (nm)	Phase
300	-	Amorphous	5	t	5	t
400	18	t	5	t	5	t
500	18	t	5	t	9	t
600	16	t	8	t	11	t
700	16	t + m	15	t	14	t + m
800	18	m	19	m	20	t + m

3.1.3. Infrared and Raman spectroscopy

The products were characterized by infrared spectroscopy in the 170-4000 cm^{-1} range. Zirconium complexes (see Fig. 4) shown a wide and intense band at 3390-3410 cm^{-1} related to asymmetric and symmetric vibrations ν(OH) [5]. Besides this, a low-intensity shoulder located at 1635-1640 cm^{-1} corresponds to the bending mode δ(HOH) of water molecules in the complexes [28]. The presence of vibration and bending modes at ~3400 cm^{-1} and ~1640 cm^{-1} suggest the presence of water molecules in a hydrogen bonds arrangements in the Zr(IV)-AcAc system, which is in agreement with the TGA/DSC results.

The IR spectra from the Zr(IV)-AcAc complexes confirmed the bidentate binding mode of the AcAc ligand to the Zr(IV) atom. The bands observed at 1553-1560 and 1335-1339 cm^{-1}, assigned to the ν(CO) and ν(C-C) of AcAc vibrations indicates chelation of acetylacetonate to the Zr(IV) center due to the shifting to lower frequencies of these two bonds: in free acetylacetone two C–O bonds give a band pattern at 1600 and 1500 cm^{-1} whereas two C–C bonds give a band pattern at 1450 and 1260 cm^{-1}. Acetylacetone is known to show tautomerism, exhibiting the keto ν(C=O) and enol ν(C=C-OH) form with peaks at 1709 and a broad band of 1640 to 1530 cm^{-1}, respectively [5,21]. The bands at 1427-1445 and 1373-1414 cm^{-1} are attributed to ν(CC) vibrations present in the PEI and PDDAC polymers, and the AcAc ligand, whereas the bands at 1036 and 846 cm^{-1} are due to bending δ(CCH), combined with ν(CC) stretch vibrations. The ν(Zr-OAcAc) vibrations appear at 450-465 cm^{-1} with an average band intensity, whereas 621-628 cm^{-1} presents bands of similar intensity due to characteristic bending vibrations ($\delta(Zr\text{-}O\text{-}H)_{br}$) of a hydroxo bridge between the metal nuclei of the Zr(IV)-AcAc complexes, as in the 930-700 cm^{-1} region there are no vibrations related to the AcAc ligand [31-32]. The $Zr\text{-}O(H)_{br}$ group exhibits bending and

stretching vibrations outside the ν(Zr-O) plane below 600 cm^{-1}, which combines with Zr-OH vibrations and superposition, so these bands are not informative [29].

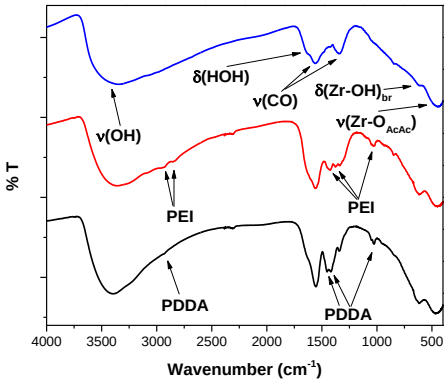

Fig. 4. FT-IR spectra for $[Zr_2(AcAc)\bullet 4H_2O]_2$ (blue), $[Zr_2(AcAc)\text{-}PEI\bullet nH_2O]_2$ (red) and $[Zr_2(AcAc)\text{-}PDDAC\bullet nH_2O]_2$ (black).

It is well known that IR spectra are very useful techniques for determining the ZrO_2 crystalline phase [33]. After calcination (Fig. 5) at 300 °C, the intensity of the water bands decreases significantly. The IR spectra of the products calcined at 800 °C present bands at 232, 263, 405, 489, 573 and 740 cm^{-1}, which are evident and can be assigned to the monoclinic phase [33-35]. Below 800 °C, with the exception of $[Zr_2(AcAc)\bullet 4H_2O]$ which also shows signs related to the monoclinic phase at 700 °C, the IR spectra show two bands of low intensity at 667 and 456 cm^{-1} related to the tetragonal zirconia phase, where the Zr atom is surrounded by eight O atoms forming a distorted cube [36]; these bands correspond to active E_u and A_{2u} of IR [37]. The tendency for an increase in the number of signals in the IR spectra, when going from one crystalline phase to another concurs because there is only one active mode in the IR for cubic ZrO_2; these active modes increase as the symmetry of the structure decreases going from cubic to tetragonal ZrO_2 and then to monoclinic ZrO_2 [21].

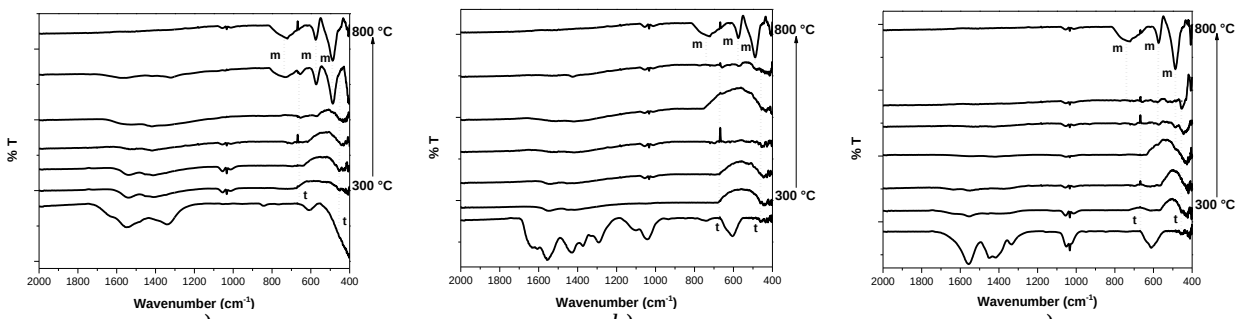

Fig. 5. FT-IR spectra for zirconium complexes and after calcination at 300-800 °C: (a) $[Zr_2(AcAc)\bullet 4H_2O]_2$, (b) $[Zr_2(AcAc)\text{-}PEI\bullet nH_2O]_2$ and (c) $[Zr_2(AcAc)\text{-}PDDA\bullet nH_2O]_2$.

Raman spectroscopy is sensitive to the polarizability of oxygen ions so it can be used to determine the symmetry of a crystalline structure. It is also recognized as a powerful tool for identifying different polymorphs of metal oxides [19,38]. According to group theory, monoclinic, tetragonal and cubic zirconia are expected to have 18 ($9A_g$ + $9B_g$), 6 ($1A_{1g}$ + $2B_{1g}$ + $3E_g$) and 3 (T_{2g}) Raman active modes, respectively [39]. Fig. 6 shows the Raman spectra of the products calcined at 800 °C of the three precursor complexes. In this figure, peaks located at 223, 303, 333, 347, 382, 475, 501, 536, 559, 615 and 638 cm^{-1} are apparent, which are characteristic of ZrO_2 in monoclinic phase. Likewise, in the case of the sample calcined at 800 °C obtained from the

$[Zr_2(AcAc)\text{-}PDDAC{\bullet}nH_2O]_2$ complex, a signal was observed at 269 cm^{-1}, which confirms the presence of the tetragonal phase combined with the monoclinic phase, concurring with the results from XRD. However, the Raman spectra for zirconium complexes and samples calcined at 300-700 °C were very low intensity due to the great fluorescence of these compounds, meaning it was not possible to identify the crystalline phases with this method.

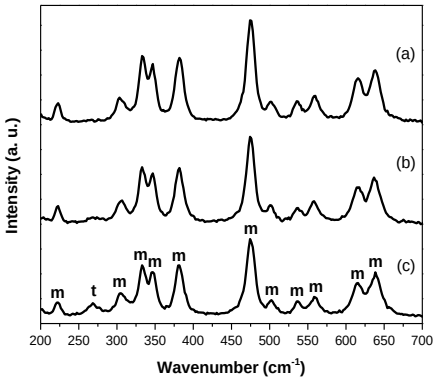

Fig. 6. Raman spectra for (a) $[Zr_2(AcAc){\bullet}4H_2O]_2$, (b) $[Zr_2(AcAc)\text{-}PEI{\bullet}nH_2O]_2$ and (c) $[Zr_2(AcAc)\text{-}PDDAC{\bullet}nH_2O]_2$ after calcination at 800 °C.

3.1.4. Diffuse Reflectance spectroscopy

The diffuse reflectance spectra, for the zirconium complexes and the zirconium oxides obtained after their calcination, are shown in Fig. 7. In the case of the $[Zr_2(AcAc){\bullet}4H_2O]$, $[Zr_2(AcAc)\text{-}PEI{\bullet}nH_2O]_2)$ and $[Zr_2(AcAc)\text{-}PDDAC{\bullet}nH_2O]_2$ response reveals an absorption band at 316 and 330 nm due LC electronic transitions $\pi \rightarrow \pi^*$ and an intense absorption band in the range of 350 to 436 nm associated to the $\pi \rightarrow \pi^*/d(Zr)$ transition; a partial metal-ligand charge-transfer character (MLCT). Likewise, these complexes show a series of shoulders in the visible region located around the 470 and 600 nm, which can be attributed to metal-ligand (ML) or ligand-metal (LM) type charge transfers, which corroborates the coordination bonding between AcAc and Zr(IV) [29,40].

Following the calcination of the complexes, the products obtained at 300 and 400 °C show a high-intensity peak located at 420 nm and a shoulder around 330 nm, which may occur due to the transition from the valence band to the conduction band [19]. At higher calcination temperatures (500-800 °C), both absorption signals decreased in intensity, due to the loss of the AcAc ligand and the PEI and PDDAC polymers, which concurs with the TGA/DSC results, and in the case of the shoulder located at 330 nm; this began to be defined as an acute maximum accompanied by a hypsochromic displacement until approximately 308 nm, whereas the band located at 420 nm shifted towards red at about 430 nm. Finally, the presence of a new low-intensity maximum, centered at 480 nm, was observed.

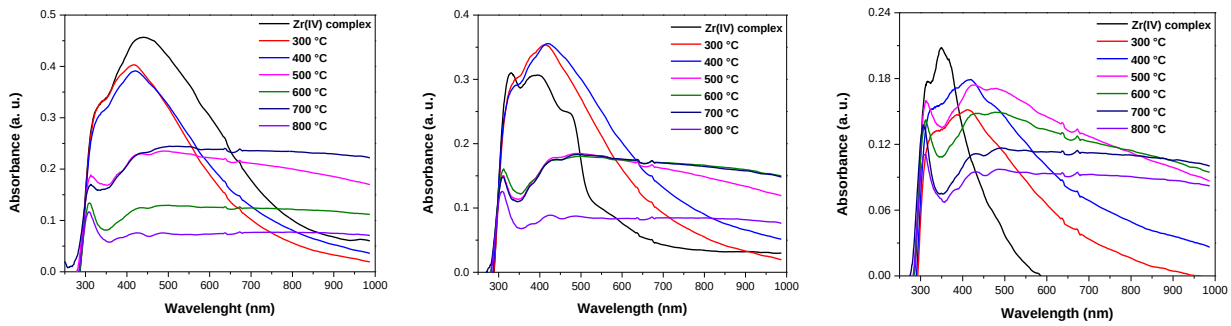

a) *b)* *c)*

Fig. 7. Diffuse reflectance spectrum of zirconium complexes and after calcination at 300-800 °C: (a) $[Zr_2(AcAc){\bullet}4H_2O]_2$, (b)$[Zr_2(Ac\ Ac)\text{-}PEI{\bullet}nH_2O]_2$ and (c) $[Zr_2(Ac\ Ac)\text{-}PDDAC{\bullet}nH_2O]_2$.

The crystalline structure of the calcinated products and the permitted direct transitions in ZrO_2 were corroborated by the relationship between $(\alpha h\nu)^2$ and $h\nu$ in the strong absorption region (Fig. 8.) [20]. The zirconium oxides obtained at temperatures of 300 and 400 °C had photon energy values in the range of 3.7 to 3.0 eV, whereas at higher temperatures (500-800 °C), these values changed to 4.0-2.9 eV. These absorption peaks for the ZrO_2 nanoparticles in the UV region manifested less energy compared to previous reports for the ZrO_2 bulk bandgap (Eg ≈ 5.0 eV), suggesting that these transitions arise from extrinsic states such as surface trap states, defect states or impurities [19]. The energies obtained for these compounds (4.0-2.9 eV) are higher than the bandgap energy of the t and m zirconia phase (2.2-2.4 eV y 3.1-3.7), previously reported [19,24]. However, the investigation showed that the apparent E_g value of t-zirconia and m-zirconia was 4.3-4.5 eV and 3.6-5.1 eV for an average particle size of 27 to 6 nm, respectively [41].

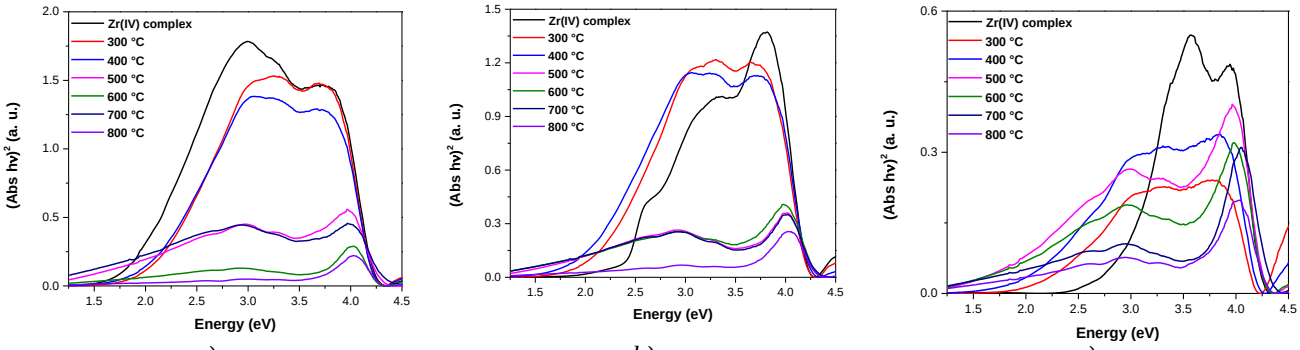

a) *b)* *c)*

Fig. 8. Tauc plots of zirconium complexes and after calcination at 300-800 °C: (a) $[Zr_2(AcAc)\bullet 4H_2O]_2$, (b) $[Zr_2(Ac\ Ac)\text{-}PEI\bullet nH_2O]_2$ and (c) $[Zr_2(Ac\ Ac)\text{-}PDDAC\bullet nH_2O]_2$.

4. Conclusions

Pure zirconium oxide nanoparticles were successfully prepared using the thermal decomposition method of three new complexes of hydrated zirconium acetylacetonate $[Zr_2(AcAc)\bullet 4H_2O]_2$, $[Zr_2(AcAc)\text{-}PEI\bullet nH_2O]_2$ and $[Zr_2(AcAc)\text{-}PDDAC\bullet nH_2O]_2$. Tetragonal and/or monoclinic zirconia nanocrystals were synthesized by calcination temperatures from 300 to 800 °C with crystallite sizes in the range of 5-20 nm.

XRD analysis showed the effect of the PEI and PDDAC stabilizers on the particle size of the products obtained after calcination, as well as the control of the crystalline phase with temperature, obtaining a tetragonal phase at low temperatures and a monoclinic phase at temperatures above 700 °C. Diffuse Reflectance spectra of the samples prepared with hydrous zirconium acetylacetonate complexes showed photon energy values (optical bandgap) in the range of 2.9 to 4.0 eV due to the extrinsic states.

Acknowledgements

This research was supported by institutional funds from the University of Guadalajara. JAPT thanks CONACyT for the scholarship.

References

[1] D. Y. Kim, C. H. Lee, S. J. Park, Journal of Materials Research **11**(10), 2583 (1996).
[2] M. Salavati-Niasari, M. Dadkhah, F. Davar, Polyhedron **28**(14), 3005 (2009).
[3] M. R. Loghman-Estarki, R. S. Razavi, H. Edris, H. Jamali, Ceramics International **40**(1), 1405 (2014).

[4] F. Davar, A. Hassankhani, M. R. Loghman-Estarki, Ceramics International **39**(3), 2933 (2013).
[5] M. Hussain, M. Mazhar, M. K. Rauf, M. Ebihara, T. Hussain, Bulletin of the Korean Chemical Society **30**(1), 92 (2009).
[6] G. Y. Guo, Y. L. Chen, Journal of Solid State Chemistry **178**(5), 1675 (2005).
[7] J. Liang, X. Jiang, G. Liu, Z. Deng, J. Zhuang, F. Li, Y. Li, Materials Research Bulletin **38**(1), 161 (2003).
[8] V. A. Sadykov, V. I. Zaikovskii, D. A. Zyuzin, E. M. Moroz, E. B. Burgina, A. V. Ishchenko, V. G. Kostrovskii, V. A. Matyshak, MRS Online Proceedings Library Archive **878** (2005).
[9] C. Stöcker, A. Baiker, Journal of Non-crystalline Solids **223**(3), 165 (1998).
[10] I. I. Štefanć, S. Musić, G. Štefanić, A. Gajović, Journal of Molecular Structure **480**, 621 (1999).
[11] J. A. Wang, M. A. Valenzuela, J. Salmones, A. Vázquez, A. Garcıa-Ruiz, X. Bokhimi, Catalysis Today **68**(1-3), 21 (2001).
[12] Y. W. Zhang, J. T. Jia, C. S. Liao, C. H. Yan, Journal of Materials Chemistry **10**(9), 2137 (2000).
[13] N. L. Wu, T. F. Wu, Journal of the American Ceramic Society **83**(12), 3225 (2000).
[14] Z. Ji, J. A. Haynes, M. K. Ferber, J. M. Rigsbee, Surface and Coatings Technology **135**(2-3), 109 (2001).
[15] S. Dosta, I. G. Cano, J. R. Miguel, J. M. Guilemany, Journal of Thermal Spray Technology **17**(3), 360 (2008).
[16] R. D. Purohit, S. Saha, A. K. Tyagi, Materials Science and Engineering: B **130**(1-3), 57 (2006).
[17] P. E. Meskin, V. K. Ivanov, A. E. Barantchikov, B. R. Churagulov, Y. D. Tretyakov, Ultrasonics sonochemistry **13**(1), 47 (2006).
[18] D. W. Johnson, American Ceramic Society Bulletin **60**(2), 221 (1981).
[19] F. Davar, M. R. Loghman-Estarki, Ceramics International **40**(6), 8427 (2014).
[20] M. Banerjee, R. W. Seidel, M. Winter, H. W. Becker, D. Rogalla, A. Devi, Dalton Transactions **43**(6), 2384 (2014).
[21] M. Salavati-Niasari, M. Dadkhah, F. Davar, Inorganica Chimica Acta **362**(11), 3969 (2009).
[22] J. Liu, J. Li, J. Wu, J. Sun, Nanoscale Research Letters **14**(1), 154 (2019).
[23] S. Seppälä, M. Vehkamäki, K. Mizohata, W. Noh, J. Räisänen, M. Ritala, M. Leskelä, Journal of Vacuum Science & Technology A: Vacuum, Surfaces, and Films **37**(2), 020912 (2019).
[24] M. Salavati-Niasari, M. Dadkhah, F. Davar, Polyhedron **28**(14), 3005 (2009).
[25] R. C. Garvie, The Journal of Physical Chemistry **69**(4), 1238 (1965).
[26] C. Huang, Z. Tang, Z. Zhang, Journal of the American Ceramic Society **84**(7), 1637 (2001).
[27] P. L. Franceschini, M. Morstein, H. Berke, H. W. Schmalle, Inorganic Chemistry **42**(22), 7273 (2003).
[28] R. Thakkar, H. Patel, U. Chudasama, Bulletin of Materials Science **30**(3), 205 (2007).
[29] I. Georgieva, N. Danchova, S. Gutzov, N. Trendafilova, Journal of Molecular Modeling **18**(6), 2409 (2012).
[30] M. Biswas, P. K. Ojha, E. M. Jayasingh, C. D. Prasad, Nanomaterials and Nanotechnology **1**, 19 (2011).
[31] S. Morris, M. J. Almond, C. J. Cardin, M. G. Drew, D. A. Rice, Y. Zubavichus, Polyhedron **17**(13), 2301 (1998).
[32] P. Tarte, Spectrochimica Acta **13**(1-2), 107 (1958).
[33] D. A. Zyuzin, S. V. Cherepanova, E. M. Moroz, E. B. Burgina, V. A. Sadykov, V. G. Kostrovskii, V. A. Matyshak, Journal of Solid State Chemistry **179**(10), 2965 (2006).
[34] C. M. Phillippi, K. S. Mazdiyasni, Journal of the American Ceramic Society **54**(5), 254 (1971).
[35] A. Feinberg, C. H. Perry, Journal of Physics and Chemistry of Solids **42**(6), 513 (1981).
[36] P. Li, I. W. Chen, J. E. Penner-Hahn, Physical Review B **48**(14), 10063 (1993).
[37] P. Bouvier, H. C. Gupta, G. Lucazeau, Journal of Physics and Chemistry of Solids **62**(5), 873 (2001).
[38] M. Angeles-Rosas, M. A. Camacho-López, E. Ruiz-Trejo, Solid State Ionics **181**(29-30),

1349 (2010).
[39] K. A. Singh, L. C. Pathak, S. K. Roy, Ceramics International **33**(8), 1463 (2007).
[40] N. Petkova, S. Dlugocz, S. Gutzov, Journal of Non-Crystalline Solids **357**(6), 1547 (2011).
[41] D. Ciuparu, A. Ensuque, G. Shafeev, F. Bozon-Verduraz, Journal of Materials Science Letters **19**(11), 931 (2000).